Hindawi
Mathematical Problems in Engineering
Volume 2019, Article ID 7876503, 9 pages
https://doi.org/10.1155/2019/7876503

Research Article

A Comparative Study of the Cracking Effect of Induced Joints of Various Spatial Formations

Haifeng Li,[1,2] **BingQi Li**,[1,2] **and Bo Yang**[1,2]

[1] *State Key Laboratory of Simulation and Regulation of Water Cycle in River Basin, Beijing 100038, China*
[2] *China Institute of Water Resources and Hydropower Research, Beijing 100038, China*

Correspondence should be addressed to Haifeng Li; lihfdlut@126.com

Received 22 August 2018; Revised 11 December 2018; Accepted 17 December 2018; Published 13 January 2019

Academic Editor: Roberto G. Citarella

The use of induced joints is a common cracking control measure used in the design of roller compacted concrete arch dams. Currently, in some projects in which radial twisted joints were used, during the construction period, some cracks appeared around the induced joints while the joints themselves failed to open. From the fracture mechanics point of view, this problem is related to the variations in the spatial formation of the induced joint planes. In this study, we formulated numerical examples involving square plate and cylindrical arch dam with joints of various planar spatial formations and used the virtual crack-closure technique and the Richard brittle fracture criterion to obtain the equivalent stress intensity factor of the joint plane, and we studied the joint plane stress intensity factor based on the variations in the joint plane formation angle. Based on the reciprocal of the normalized stress intensity factor, we obtained the equivalent strength correction coefficient for induced joints of varying plane angles, referred to in this study as the joint plane formation factor $\psi(\alpha)$, in order to reflect the influence of varying joint plane formations on the induced joint cracking. Our study results show that as the joint plane angle continuously increases, it is more difficult for the induced joints to open, which implies a gradual increase in the equivalent strength of the joint plane. Therefore, in the actual design of rolled concrete arch dams, the straight transverse joint layout should be used for induced joints. If the use of the radial twisted joint layout is necessary, the joint plane angle should not exceed 10°.

1. Introduction

In the roller compacted concrete (RCC) arch dam projects, the planes of transverse joints and induced joints are generally planar, folded, or curved [1]; considering their spatial formation, the planar induced joints are straight transverse joints, while folded and curved joints can be considered radial twisted joints (see Figure 1). At present, in some projects that use radial twisted joints, a phenomenon has been observed in which some cracks appear around the induced joints before their opening and prior to the impoundment of the dam. For example, this problem occurred in an RCC arch dam located in the southwest China, where the radial twisted joint layout was employed for induced joints (see Figure 2 for details). In view of this phenomenon, some researchers have proposed that radial twisted joints are not conducive to the normal opening of induced and transverse joints in RCC arch dams. Therefore, a comparative study on the effect of various joint plane formations on the induced joint cracking is needed.

At present, most experimental research on induced joint cracking focuses on the weakened areas of the induced planes. The equivalent strength model created by Professor Zeng Zhaoyang [2] accounted for the cracking effect of induced joints at a structural level and found that the cracking size was related not only to the material itself, but also directly to the shape, size, and the layout of joints. However, the model did not take into consideration the influence of the joint plane formation. In addition, some researchers have studied the problem of noncoplanar induced joint layout based on fracture mechanics [3] and discussed the feasibility of an oblique layout of induced joints but have simplified the noncoplanar induced joint cracking into two planar problems: within the horizontal plane and within the vertical plane perpendicular to the radial direction. This approach

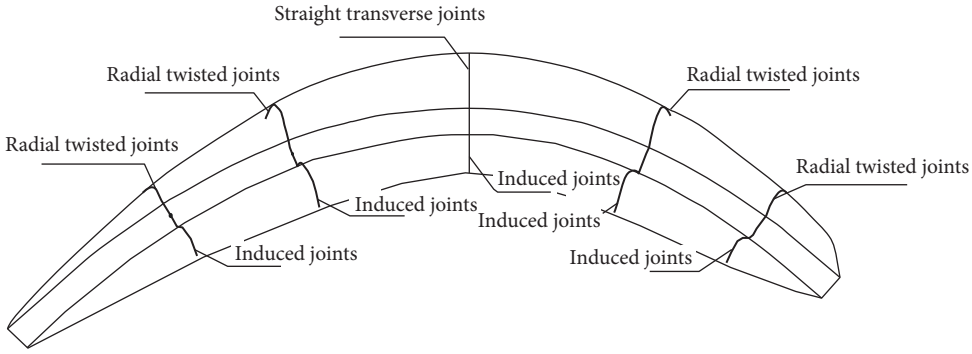

Figure 1: Spatial morphology diagram of the induced joints.

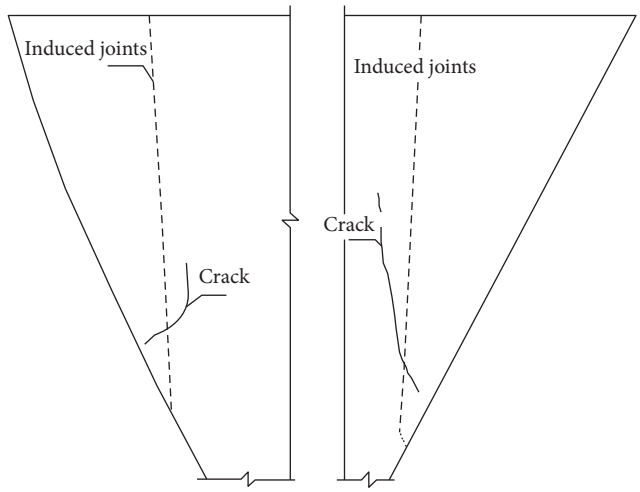

Figure 2: Diagram of downstream dam surface cracks of some RCC Arch Dam in southwest China.

cannot effectively reflect the spatial effect of the noncoplanar induced joint cracking problem. Strictly speaking, induced joint cracking is a three-dimensional fracturing problem; many scholars have made many research achievements in this field [4–8]. Therefore, a three-dimensional approach is necessary in order to analyze the stress on the induced joints of various spatial formations and to study the cracking effect of various joint plane formations of induced joints.

Based on stress variation characteristics of roller compacted concrete arch dam and the cracking variation patterns of induced joints, in this article we formulated numerical examples involving finite square plate and cylindrical arch dam with joint planes of various spatial formations and used the virtual crack-closure technique to study the variation patterns of fracture parameters under different loading conditions. Based on the Richard brittle fracture criterion [9], we obtained the equivalent stress intensity factor of spatial joints and studied the stress intensity factor based on changes in the joint formation angle. Based on the reciprocal of the normalized stress intensity factor, we obtained the equivalent strength correction coefficients for induced joint planes of various angles, in order to reflect the influence of various joint plane spatial formations on the induced joint cracking.

2. Joint Surface Cracking Parameter Determination Methodology

2.1. Virtual Crack-Closure Method for Surface Cracks. At present, the main method for the determination of the stress intensity factor [10] is through direct extrapolation based on the displacement or the stress near the tip of the crack. In order to improve the accuracy of the results, singular element is often used. In addition, by using the equivalent area integrals, such as the J- or M-integral, near the crack tip, or by employing the virtual crack-closure method [11, 12] to obtain the energy release rate, the stress intensity factor is obtained through transformation. In view of its simplicity and reliable accuracy, in this study we used the virtual crack-closure method to obtain the cracking parameters of surface cracks.

Since the induced joints can be treated as unispatial surface cracks, the virtual crack propagation method is used to calculate the strain release rate with the following formula:

$$G_{\mathrm{I}} = \lim_{\Delta a \longrightarrow 0} \frac{1}{2\Delta A} \int_{\Delta A} \overline{\sigma}_{zz}^{(1)} (\Delta a - r, 0) \cdot \Delta \overline{w}^{(2)} (r, \pi)\, dxdy$$

$$G_{\mathrm{II}} = \lim_{\Delta a \longrightarrow 0} \frac{1}{2\Delta A} \int_{\Delta A} \overline{\tau}_{xz}^{(1)} (\Delta a - r, 0) \cdot \Delta \overline{u}^{(2)} (r, \pi)\, dxdy$$

$$G_{\mathrm{III}} = \lim_{\Delta a \longrightarrow 0} \frac{1}{2\Delta A} \int_{\Delta A} \overline{\tau}_{yz}^{(1)} (\Delta a - r, 0) \cdot \Delta \overline{v}^{(2)} (r, \pi)\, dxdy \tag{1}$$

where G_{I}, G_{II}, and G_{III} are the strain release rate components of the three types of cracks, respectively; ΔA is the surface area of the virtual crack extension along the leading edge of the actual crack tip; $\overline{\sigma}_{zz}^{(1)}(\Delta a - r, 0)$, $\overline{\tau}_{xz}^{(1)}(\Delta a - r, 0)$, and $\overline{\tau}_{yz}^{(1)}(\Delta a - r, 0)$ are the stress components of the virtual crack extension line along the leading edge of the actual crack tip; $\Delta \overline{u}^{(2)}(r, \pi), \Delta \overline{v}^{(2)}(r, \pi)$, and $\Delta \overline{w}^{(2)}(r, \pi)$ are the opening displacement components of the virtual crack extension line along the back of the virtual crack tip.

2.2. Energy Release Rate and Stress Intensity Factor Transformation. After using the three-dimensional virtual crack-closure method to obtain the energy release rate, (2) should be used to calculate the three-dimensional stress intensity factor.

$$K_{\mathrm{I}} = \sqrt{G_{\mathrm{I}} E}$$

$$K_{\mathrm{II}} = \sqrt{G_{\mathrm{II}} E} \tag{2}$$

$$K_{\mathrm{III}} = \sqrt{\frac{G_{\mathrm{III}} E}{1 + \nu}}$$

where K_{I}, K_{II}, and K_{III} are the stress intensity factors of the three types of cracks, respectively; G_{I},G_{II}, and G_{III} are the strain release rate components of the three types of cracks, respectively; E is the elastic modulus of the material; ν is the Poisson ratio of the material.

2.3. Equivalent Stress Intensity Factor. As mentioned above, strictly speaking, induced joint cracking is a three-dimensional fracturing problem. Currently, no unified theoretical criterion exists for the mixed-mode (I+III, I+II, II+III, and I+II+III type) fracture problems due to the complexity of the mathematical calculations and difficulty in experimentation. In the recent 30 years, the Pook criterion [13] and the Richard criterion [14] have been the most influential three-dimensional mixed-mode fracture criteria. Even though the twisting angle ψ_0 of the Pook criterion takes into consideration the three types of stress intensity factors K_{I}, K_{II}, and K_{III}, however, the deflection angle φ_0 used in the criterion is not related to the mode III stress intensity factor K_{III}. Richard considers this as inconsistent with the actual conditions of three-dimensional fractures. Therefore, this study uses the Richard criterion to obtain the equivalent stress intensity factor of joint planes.

The Richard criterion is essentially the maximum principal stress criterion, expressed as σ_1'. This criterion assumes that the cracks extend in the direction perpendicular to the maximum principal stress σ_1'. However, because the series of theoretical formulas of the σ_1' criterion are too complex and inconvenient to calculate, Richard simplifies the theoretical formulas and establishes the crack condition analysis and the initial crack angle equations.

The Richard criterion deflection angle φ_0 equation is as follows:

$$\varphi_0 = \mp \left[A \frac{|K_{\mathrm{II}}|}{K_{\mathrm{I}} + |K_{\mathrm{II}}| + |K_{\mathrm{III}}|} + B \left(\frac{|K_{\mathrm{II}}|}{K_{\mathrm{I}} + |K_{\mathrm{II}}| + |K_{\mathrm{III}}|} \right)^2 \right] \tag{3}$$

where φ_0 is the deflection angle of surface cracks; when $K_{\mathrm{II}} > 0$, $\varphi_0 < 0^0$; when $K_{\mathrm{II}} < 0$, $\varphi_0 > 0^0$; A, B are the calculation coefficients.

The twisting angle ψ_0 equation is as follows:

$$\psi_0 = \pm \left[C \frac{|K_{\mathrm{III}}|}{K_{\mathrm{I}} + |K_{\mathrm{II}}| + |K_{\mathrm{III}}|} + D \left(\frac{|K_{\mathrm{III}}|}{K_{\mathrm{I}} + |K_{\mathrm{II}}| + |K_{\mathrm{III}}|} \right)^2 \right] \tag{4}$$

where ψ_0 is the twisting angle of surface cracks; when $K_{\mathrm{III}} > 0$, $\psi_0 < 0^0$; when $K_{\mathrm{III}} < 0$, $\psi_0 > 0^0$; C, D are the calculation coefficients.

The calculation coefficients $A = 140^0$, $B = -70^0$, $C = 78^0$, $D = -33^0$.

The equation for the I+II+III mixed-mode equivalent stress intensity factor $K_{eff-\mathrm{I,II,III}}$ is as follows:

$$K_{eff-\mathrm{I,II,III}} = \frac{K_{\mathrm{I}}}{2} + \frac{1}{2} \sqrt{K_{\mathrm{I}}^2 + 4 (\alpha_1 K_{\mathrm{II}})^2 + 4 (\alpha_2 K_{\mathrm{III}})^2} \tag{5}$$

where α_1 is the ratio of $K_{\mathrm{IC}}/K_{\mathrm{IIC}}$, α_2 is the ratio of $K_{\mathrm{IC}}/K_{\mathrm{IIIC}}$, with K_{IC}, K_{IIC}, and K_{IIIC} as the fracture toughness for modes I, II, and III. Richard assumes that $\alpha_1 = 1.155$, and $\alpha_2 = 1.0$.

3. A Comparison of the Cracking Effect of Induced Joints with Various Spatial Formation

3.1. Comparative Analysis of Square Plate

(1) Computation Model. A 30x30m square plate with a thickness of 5 m was set up. A series of 3-meter long, penetrated induced joints were created along the central axis of the plate at 3-meter intervals. The angle α between the joints was set at 0°, 5°, 7.5°, 10°, 12.5°, 15°, 20°, 25°, and 30°. The plate was loaded on both sides and two types of loading conditions were considered: an axial tensile loading and a compressive shear loading. The corresponding computation model is shown in Figure 3.

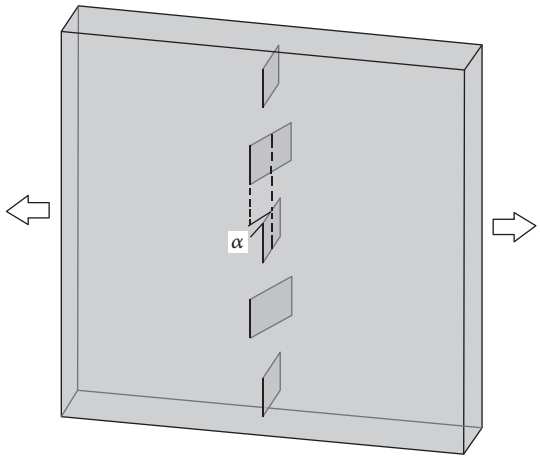

Figure 3: The computation model of square plate.

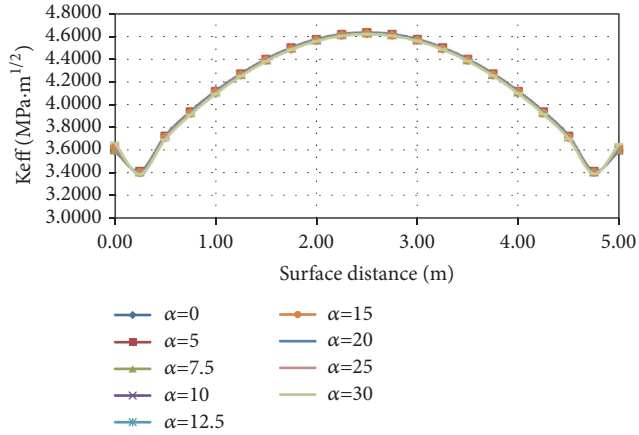

Figure 4: Distribution curve of the stress intensity factors of the front edge of straight joints along the thickness direction under axial tensile load.

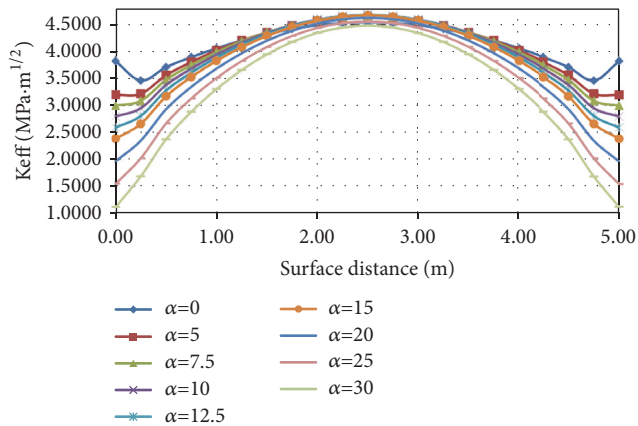

Figure 5: Distribution curve of the stress intensity factors of the front edge of twisted stitches along the thickness direction under compression-shear load.

(2) Results Analysis

(1) Variation Patterns of Joint Plane Stress Intensity Factors. Using the virtual crack-closure technique, the energy release rate of each node at the front edge of the crack under different loads can be obtained. The equivalent stress intensity factor at the front edge of the joint plane can be obtained after altering (2) and (5). The distribution curve of the stress intensity factor along the thickness direction under different loads (see Figures 4-5) shows that as the angle between the transverse joints and the twisted joints gradually increases, the equivalent stress intensity factor along the front edge of the joint gradually decreases. The change in the equivalent stress intensity factor of the transverse joints was minimal, while decrease in the equivalent stress intensity factor of twisted joints was more significant.

(2) The Equivalent Stress Intensity Factor Variation Patterns for Various Joint Plane Angles. In order to facilitate the comparative analysis of the stress intensity factors of various joint plane angles, the front edge equivalent stress intensity factors of the joints were averaged, as shown in Table 1. Generally, the average equivalent stress intensity factor of the joint decreases as the joint plane angle increases, and the reduction trend under the shear loading is greater than that of the axial loading.

In order to study the variations between the stress intensity factor and the changing joint plane angle, the transverse and twisted joint angle of 0° was set as the benchmark. The average equivalent stress intensity factor values for various joint plane angles were normalized. The variation curves are shown in Figures 6-7. The normalized variation curves show that as the joint plane angle increases, the equivalent stress intensity factor of the transverse joint essentially remains the same, while that of the twisted joint is significantly reduced.

Under the axial tensile loading, when the joint plane angle increased to 25°, the twisted joint plane stress intensity factor was reduced only by 2%. At the same time, under the compressive shear loading, when the joint plane angle was 5°, the twisted joint plane stress intensity factor decreased by 2%; when the angle increased to 10°, the factor decreased by 4.3%; when the angle increased to 15°, the factor decreased by 7.5%; when the angle increased to 25°, the factor decreased by 16%; when the angle increased to 30°, the factor decreased by 21%.

Generally speaking, as the joint plane angle increases, the stress intensity factor of the joint plane decreases by varying degrees, and the decrease of the twisted joint factor was significantly larger than that of the transverse joint. When the joint plane angle was 10°, the maximum decrease in the stress intensity factor was 4.3%; at a 20° angle, the maximum decrease was 11.4%; at a 25° angle, the maximum decrease was 16%; at a 30° angle, the maximum decrease was 21%.

3.2. Comparative Analysis of Cylindrical Arch Dam

(1) Computation Model. For RCC arch dams, the induced joints are usually located in the bank section. In case of induced joints, consideration should be given to the stress conditions of the arch dam before its first impoundment. This is due to the fact that before the completion of the

Table 1: Summary of average equivalent stress intensity in the crack front edge of a finite plate with different seam surface angles.

Load	location	0°	5°	7.5°	10°	12.5°	15°	20°	25°	30°
Axial tensile load	Crack tip for transverse joint	2.571	2.571	2.571	2.571	2.571	2.571	2.571	2.570	2.569
	Crack tip for twisted joint	2.552	2.552	2.551	2.550	2.548	2.545	2.531	2.505	2.367
Compression-shear load	Crack tip for transverse joint	4.144	4.141	4.140	4.138	4.137	4.135	4.133	4.132	4.130
	Crack tip for twisted joint	4.119	4.038	3.995	3.942	3.880	3.810	3.649	3.464	3.259

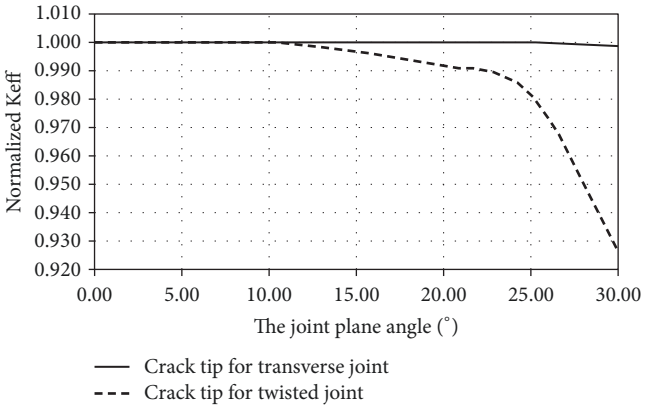

Figure 6: Variation of the average equivalent stress intensity factors with the joint angle change of the front edge of the crack under axial tensile load.

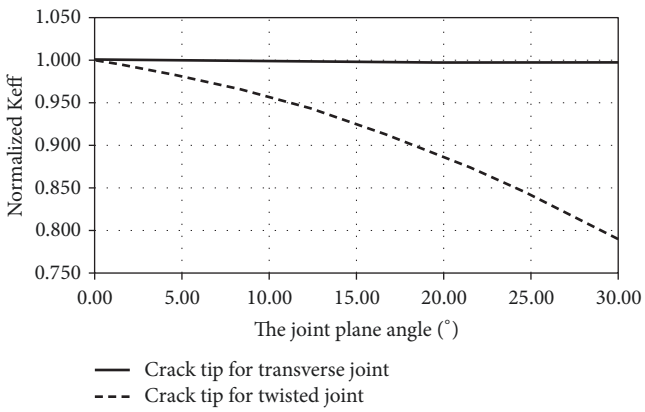

Figure 7: Variation of the average equivalent stress intensity factors with the joint angle change of the front edge of the crack under compression-shear load.

impoundment, arch dams are normally in a state of tensile stress due to the construction temperature drop, which is conducive to the opening of the induced joints. This is the optimal time for the effective functioning of induced joints. If the induced joints do not open before the impoundment, after the impoundment, the arch dam is generally under stress due to the loading effect of the upstream water, which makes it very difficult for the induced joints to open and function effectively [15].

Based on the above analysis, a semicylindrical arch dam model with a thickness of 5 m, an inner diameter of 60 m, an outer diameter of 65 m, a height of 27 m, and a semicentral angle of 45° was set up. The bank slope was taken into consideration. The model was set up in a trapezoidal form. Slope angles β of 30°, 45°, and 60° were considered. Series of 3-meter long, penetrated induced joints were created at 3-meter intervals, at 1/3 of the total height from the base. The angle α between joints was set at 0°, 5°, 7.5°, 10°, 12.5°, 15°, 20°, 25°, and 30°. Figure 8 shows the detailed model. The temperature drop of 5° was taken into consideration for the loading conditions. The two sides of the semicylindrical arch dam were constrained, the left side being fully constrained by the bank, and the right side being constrained symmetrically.

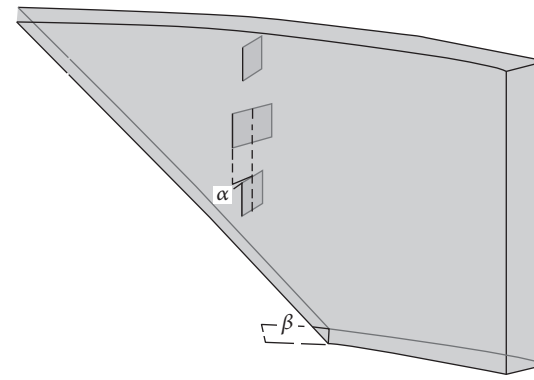

Figure 8: The computation model of cylindrical arch dam.

(2) Results Analysis. In order to facilitate the comparative analysis of the stress intensity factor of various joint plane angles, the equivalent stress intensity factors of the front edges of the joint planes were averaged, as shown in Table 2. Generally, as the joint plane angle increases, the average equivalent stress intensity factor of the joint plane decreases correspondingly. In order to study the variations between the stress intensity factor and the changing joint plane angle, the angle of 0° between the transverse and twisted joints was set as the benchmark. The average equivalent stress intensity factor values for various joint plane angles were normalized. The variation curves are shown in Figures 9–11.

The normalized equivalent stress intensity factor variation curves show that as the joint plane angle increases, the decrease in the stress intensity factor of the twisted joint plane is more significant than that of the transverse joint plane. At a slope of 30°, and when the joint plane angle increased to 5°, the stress intensity factor of the transverse and twisted joint planes decreased by 1%; at a 10° angle, the factor decreased by 2%; at a 20° angle, the stress intensity factor of the transverse joint decreased by 2.5%, while that of the twisted joint decreased by 5%; at a 25° angle, the transverse

Table 2: Summary of average equivalent stress intensity in the crack front edge of a cylindrical arch dam of different seam surface angles.

Slope angles	Location	0°	5°	7.5°	10°	12.5°	15°	20°	25°	30°
30°	Crack tip for transverse joint	1.175	1.166	1.163	1.160	1.157	1.156	1.143	1.141	1.132
	Crack tip for twisted joint	1.672	1.658	1.650	1.642	1.631	1.622	1.581	1.530	1.445
45°	Crack tip for transverse joint	0.770	0.770	0.770	0.759	0.756	0.755	0.758	0.752	0.726
	Crack tip for twisted joint	1.211	1.191	1.181	1.170	1.158	1.147	1.112	1.077	1.036
60°	Crack tip for transverse joint	0.807	0.806	0.805	0.805	0.752	0.751	0.746	0.739	0.733
	Crack tip for twisted joint	1.067	1.058	1.053	1.047	1.021	1.012	0.995	0.939	0.886

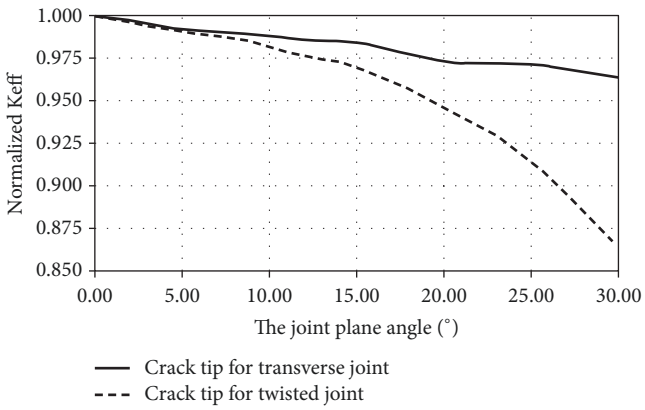

Figure 9: Variation of the average equivalent stress intensity factors with the joint angle change of the front edge of the crack with the slope angel 30 degrees.

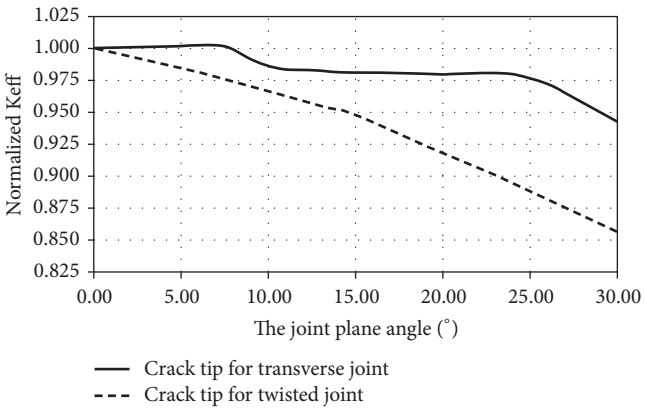

Figure 10: Variation of the average equivalent stress intensity factors with the joint angle change of the front edge of the crack with the slope angel 45 degrees.

factor decreased by 3%, while the twisted factor decreased by 8.5%; at a 30° angle, the transverse factor decreased by 3.5%, while the twisted factor by 14%.

When the slope increased to 45° while the joint plane angle was 5°, the transverse joint remained unchanged, while the twisted joint decreased by 1.5%; at a 10° angle, the transverse joint decreased by 1.5%, while the twisted joint decreased by 3.3%; at a 15° angle, the transverse joint

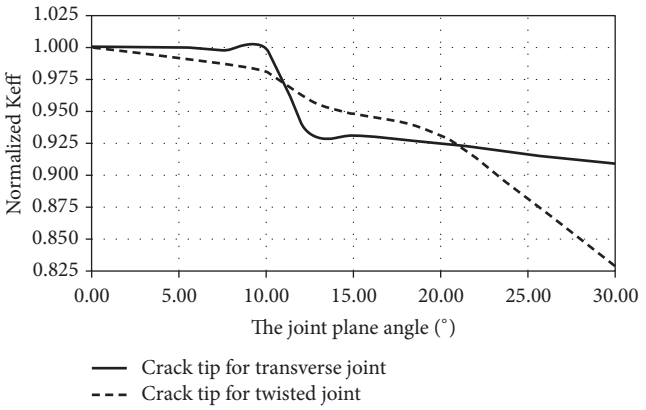

Figure 11: Variation of the average equivalent stress intensity factors with the joint angle change of the front edge of the crack with the slope angel 60 degrees.

decreased by 2%, while the twisted joint decreased by 5%; at a 20° angle, the transverse joint decreased by 2%, while the twisted joint decreased by 8%; at a 25° angle, the transverse joint decreased by 2.3%, while the twisted joint decreased by 11%; at a 30° angle, the transverse joint decreased by 5.7%, and the twisted joint decreased by 14%.

When the slope increased to 60°, while the joint plane angle was 10°, the transverse joint remained practically unchanged, while the twisted joint decreased by 2%; at a 15° angle, the transverse joint decreased by 7%, while the twisted joint decreased by 5%; at a 20° angle, the transverse joint decreased by 7.5%, while the twisted joint decreased by 7%; at a 25° angle, the transverse joint decreased by 8.4%, while the twisted joint decreased by 12%; at a 30° angle, the transverse joint decreased by 9%, while the twisted joint decreased by 17%.

Generally speaking, as the joint plane angle increases, the stress intensity factor of the joint plane decreases by varying degrees, and the decrease of the twisted joint is significantly larger than that of the transverse joint. When the joint plane angle is at 10°, the stress intensity factor decreases by a maximum of 3%. When the joint plane angle is at 20°, the maximum decrease of the stress intensity factor is by 8%. When the joint plane angle is at 25°, the maximum decrease of the stress intensity factor is by 12%. When the joint angle is at 30°, the maximum decrease of the stress intensity factor is by 17%.

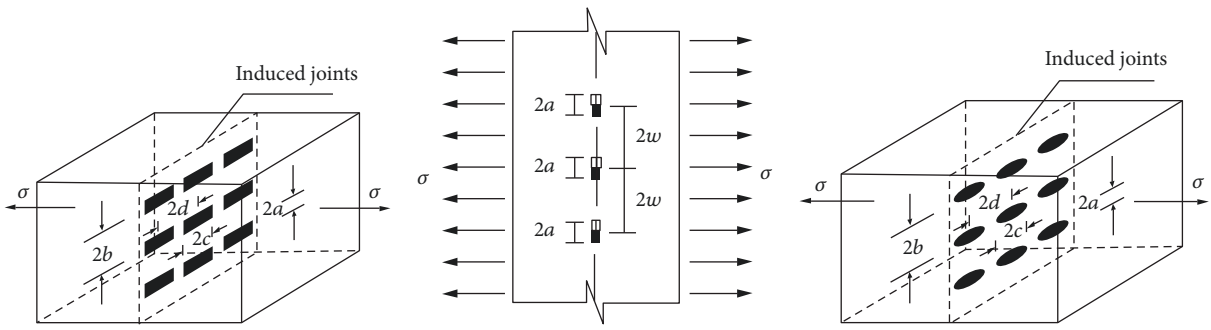

(a) Calculation diagram (b) The infinite plate penetrating crack model (c) The infinite generally buried elliptical model

Figure 12: The computation model of induced joints.

4. Discussion and Modification of the Existing Equivalent Strength Model of Induced Joints

In order to study the problem of the induced joint cracking and the optimal arrangement of induced joints, Professor Zeng Zhaoyang simplified the induced joint problem into the infinite plate penetrating crack model and the elliptical crack embedded in an infinite body model (Figure 12). According to Zhang Xiaogang et al. [16], the induced joint equivalent strength models obtained using these two computation models are similar. The model of the elliptical crack embedded in an infinite body can account for both the influence along the minor axis of adjacent induced joints and the far field stress σ and for the induced joint minor axis effective crack length. Therefore, at present, most equivalent strength equations for induced joints adopt the equivalent intensity calculation model based on the elliptical crack embedded in an infinite body, as shown in

$$
\begin{aligned}
f_{eq} &= \frac{\Phi \cdot K_{1C}}{\gamma\sqrt{\pi\left(a + r_0\right)}} \\
\gamma &= \sqrt{\frac{2b}{\pi\left(a + r_0\right)} \tan\frac{\pi\left(a + r_0\right)}{2b}} \\
r_0 &= \frac{1}{\pi}\left(\frac{K_{1C}}{f_t}\right)^2 \\
\Phi &= \int_0^{\pi/2} \left(\sin^2\theta + \frac{a^2}{c^2}\cos^2\theta\right)^{1/2} d\theta
\end{aligned}
\tag{6}
$$

where f_{eq} is the equivalent strength of the induced joint, K_{1C} is the fracture toughness of concrete, γ is the correction factor that reflects the interaction between the adjacent reserved secondary joints, r_0 is the concrete strain softening parameter related to the region dimensions, Φ is the second elliptic integral, θ is the direction angle, starting with the long axis, and a, b, c are the dimensions and interval spacing of the subjoints shown in Figure 12.

Based on the double-K fracture theory of concrete [17–20], Song Yupu, Huang Dahai [21], Zhang Xiaogang [22], Liu Haicheng [23], Huang Zhiqiang [24], Wang Xuezhi [25, 26], and other scholars from the Dalian University of Technology carried out induced joint cracking tests under varying conditions. The induced joint equivalent strength theory was modified based on the various experimental aspects, including the induced plane type, the sample size effect, the boundary effect, the effective expansion of the crack, and the nominal fracture toughness of concrete. However, the above modifications did not account for the influence of the joint plane spatial formation on the equivalent strength model of induced joints. The square plate and the cylindrical arch dam analysis results show that as the joint plane angle increases, the joint plane stress intensity factor decreases by varying degrees. Moreover, the decrease in the twisted joints is significantly greater than that of the transverse joints. The normalized joint plane stress intensity factors under various conditions are listed in columns (1)~(5) of Table 3. As a safety margin, the minimum stress intensity factor values from the first (5) columns are shown in part (6). The data in column (6) shows that when the joint plane angle is 5°, the joint plane stress intensity factor decreases to 0.98; when the angle is 10°, the factor decreases to 0.957; when the angle is 15°, the factor decreases to 0.925; when the angle is 20°, the factor decreases to 0.886; and when the angle is 30°, the factor decreases to 0.791.

From the viewpoint of the induced joint equivalent strength theory, as the joint plane angle continues to increase, it becomes more difficult for the joints to open, which implies a gradual increase of the joint plane equivalent intensity. Therefore, the reciprocal of the normalized stress intensity factor can be used as the correction coefficient of the induced joint equivalent strength for various joint plane angles, which is referred in this study as the spatial formation factor of the joint plane $\psi(\alpha)$.

As a safety factor, the reciprocal of the normalized stress intensity factor shown in part (6) of Table 3 is used as the joint plane spatial formation factor, as shown in part (7). The distribution curve (Figure 13) of the joint plane spatial formation factor of various joint plane angles shows that as the angle continuously increases, the equivalent strength of the twisted joint plane also increases; when the angle is 5°, the joint plane spatial formation factor is 1.02, which means that

Table 3: Summary of average equivalent stress intensity factor and spatial morphology impacting factor of different seam surface angles.

The joint plane angle	Normalized $K_{eff-\mathrm{I,II,III}}$						The spatial formation factor of the joint plane $\psi(\alpha)$
	(1)	(2)	(3)	(4)	(5)	(6)	
0.0	1.000	1.000	1.000	1.000	1.000	1.000	1.00
5.0	1.000	0.980	0.991	0.984	0.992	0.980	1.02
7.5	1.000	0.970	0.987	0.976	0.987	0.970	1.03
10.0	1.000	0.957	0.982	0.967	0.981	0.957	1.04
12.5	0.999	0.942	0.975	0.956	0.957	0.942	1.06
15.0	0.997	0.925	0.970	0.948	0.948	0.925	1.08
20.0	0.992	0.886	0.946	0.918	0.932	0.886	1.13
25.0	0.982	0.841	0.915	0.890	0.880	0.841	1.19
30.0	0.927	0.791	0.864	0.856	0.830	0.791	1.26

Note: (1) is the average equivalent stress intensity factor of the twisted joint plane in a square plate under uniaxial tensile loading; (2) is the average equivalent stress intensity factor of the twisted joint plane in a square plate under shear loading; (3) is the average equivalent stress intensity factor of the twisted joint plane in a semicylindrical arch dam with the slope angle of 30° under temperature drop loading; (4) is the average equivalent stress intensity factor of the twisted joint plane in a semicylindrical arch dam with the slope angle of 45° under temperature drop loading; (5) is the average equivalent stress intensity factor of the twisted joint plane of in semicylindrical arch dam with the slope angle of 60° under temperature drop loading; (6) is the lowest value of the normalized stress intensity factor shown in columns (1)~(5); (7) is the joint plane spatial formation factor.

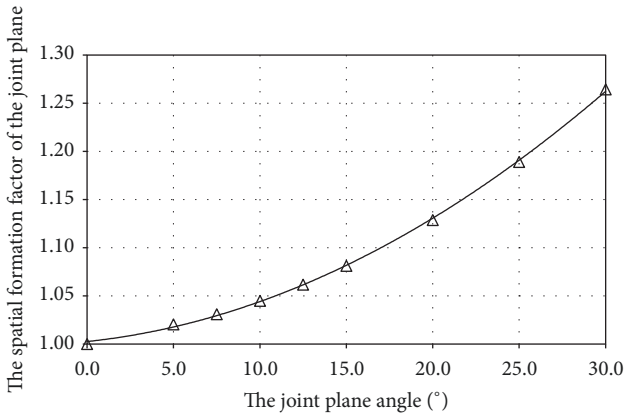

Figure 13: Spatial morphology impacting factors of seam surfaces of different intersection angles.

the induced joint equivalent strength increases by 2%; when the angle is 10°, the equivalent strength increases by 4%; when the angle is 15°, the equivalent strength increases by 8%; when the angle is 20°, the equivalent strength increases by 13%; and when the angle is 30°, the equivalent strength increases by 26%.

In order to facilitate its application in design, we used a regression fit function on the joint plane spatial formation factor of various plane angles, and we were able to obtain a best-fit equation, shown as (7), with the correlation coefficient of 0.9995.

$$\psi(\alpha) = 0.0002 \times \alpha^2 + 0.0019 \times \alpha + 1.0026 \tag{7}$$

where $\psi(\alpha)$ is the joint plane spatial formation factor and α is the induced joint plane angle.

Based on the above analysis, we can add the joint plane spatial formation factor to the equivalent strength model of induced joints to reflect its influence on the equivalent strength, as shown in

$$f_{eq} = \frac{\Phi \cdot K_{1C}}{\gamma\sqrt{\pi\left(a + r_0\right)}} \cdot \psi(\alpha) \tag{8}$$

5. Conclusions

Based on the analysis presented above, the following conclusions can be drawn from the study:

(1) As the joint plane angle increases, in all cases, the joint plane stress intensity factor decreases by varying degrees. Moreover, the twisted joint decrease is more significant than that of the transverse joint. When the joint plane angle was 10°, the maximum decrease in the stress intensity factor was 4.3%; at a 20° angle, the maximum decrease was 11.4%; at a 25° angle, the maximum decrease was 16%; at a 30° angle, the maximum decrease was 21%.

(2) Taking into consideration the induced joint equivalent strength theory, as the joint plane angle continues to increase, it is more difficult for the joint planes to open, which implies a gradual increase of the joint plane equivalent strength. The reciprocal of the normalized stress intensity factor can be used as the correction coefficient for the equivalent strength factor of induced joints of various plane angles, which is referred to as the joint plane spatial formation factor $\psi(\alpha)$, to reflect the influence of various joint plane spatial formations on the induced joint equivalent strength.

(3) As the joint plane angle continues to increase, the equivalent strength of the twisted joint plane also gradually increases. Therefore, the joint plane spatial formation factor can be added to the existing equivalent strength model of induced joints to reflect the influence of the joint plane spatial formation on the equivalent strength, as shown in (8).

(4) When the joint plane angle exceeds 10°, the induced joint equivalent strength increases by more than 4%, which

is not conducive to the opening of the joints and will lead to joint plane roughness and influence the quality of repeated grouting. At present, the existing design of twisted joints does not exceed 10°. To summarize the above analysis, the transverse joint layout should be used in the design of induced joints. If the use of twisted joints is necessary, the joint plane angle should not exceed 10°.

Data Availability

The data used to support the findings of this study are available from the corresponding author upon request.

Conflicts of Interest

The authors declare that there are no conflicts of interest regarding the publication of this article.

Acknowledgments

This work was supported by the National Natural Science Foundation of China (Grant Nos. 51779276, 51779277, and 51579252).

References

[1] F. Fang, Q. Long, H. Luo et al., *Technology and Practice of Rolling Concrete Dam in Canyon Area*, Water & Power Press, Beijing, China, 2015.

[2] Z. Zeng and Q. Ma, *Study on the structural joints in the high RCC arch dam*, Water Power, 1998.

[3] L. I. Haifeng, B. Yang, G. Zhang et al., "Study on several key problems about anti-cracking design of induced joints in RCC archdams," *Journal of Hydraulic Engineering*, vol. 49, no. 3, pp. 343–352, 2018.

[4] V. Giannella, M. Perrella, and R. Citarella, "Efficient FEM-DBEM coupled approach for crack propagation simulations," *Theoretical and Applied Fracture Mechanics*, vol. 91, pp. 76–85, 2017.

[5] M. Perrella, V. P. Berardi, and G. Cricrì, "A novel methodology for shear cohesive law identification of bonded reinforcements," *Composites Part B: Engineering*, vol. 144, pp. 126–133, 2018.

[6] G. Zhang, X. Li, and H. Li, "Simulation of hydraulic fracture utilizing numerical manifold method," *Science China Technological Sciences*, vol. 58, no. 9, pp. 1542–1557, 2015.

[7] R. Dimitri, N. Fantuzzi, Y. Li, and F. Tornabene, "Numerical computation of the crack development and SIF in composite materials with XFEM and SFEM," *Composite Structures*, vol. 160, pp. 468–490, 2017.

[8] N. Fantuzzi, R. Dimitri, and F. Tornabene, "A SFEM-based evaluation of mode-I Stress Intensity Factor in composite structures," *Composite Structures*, vol. 145, pp. 162–185, 2016.

[9] M. Schöllmann, H. A. Richard, G. Kullmer, and M. Fulland, "A new criterion for the prediction of crack development in multiaxially loaded structures," *International Journal of Fracture*, vol. 117, no. 2, pp. 129–141, 2002.

[10] D. Xie, Q. Qian, and L. Changan, *Numerical Calculation Method and Engineering Application of Fracture Mechanics*, Science Press, Beijing, China, 2009.

[11] E. F. Rybicki and M. F. Kanninen, "A finite element calculation of stress intensity factors by a modified crack closure integral," *Engineering Fracture Mechanics*, vol. 9, no. 4, pp. 931–938, 1977.

[12] K. N. Shivakumar, P. W. Tan, and J. C. Newman Jr., "A virtual crack-closure technique for calculating stress intensity factors for cracked three dimensional bodies," *International Journal of Fracture*, vol. 36, no. 3, pp. R43–R50, 1988.

[13] L. P. Pook, *Linear Elastic Fracture Mechanics for Engineers: Theory and application*, WIT Press, Southampton, 2000.

[14] H. A. Richard, M. Sander, M. Fulland, and G. Kullmer, "Development of fatigue crack growth in real structures," *Engineering Fracture Mechanics*, vol. 75, no. 3-4, pp. 331–340, 2008.

[15] G.-X. Zhang, B. Yang, and J.-H. Zhang, "Grouting temperature and thermal load of RCC arch dam," *Journal of Hydraulic Engineering*, vol. 42, no. 7, pp. 812–818, 2011.

[16] Z. XiaoGang, *The experimental study and numrical simulation on strength and fracture of induced crack in roller compacted concrete*, Dalian University of Technology, China, 2005.

[17] S. Xu and H. W. Reinhardt, "Determination of double-*K* criterion for crack propagation in quasi-brittle fracture, part I: experimental investigation of crack propagation," *International Journal of Fracture*, vol. 98, no. 2, pp. 111–149, 1999.

[18] S. Xu and H. W. Reinhardt, "Determination of double-K criterion for crack propagation in quasi-brittle fracture, part II: analytical evaluating and practical measuring methods for three-point bending notched beams," *International Journal of Fracture*, vol. 98, no. 2, pp. 151–177, 1999.

[19] S. Kumar and S. V. Barai, "Crack propagation study using double- K, and double- G, fracture parameters," in *Concrete Fracture Models and Applications*, Springer, Berlin, Germany, 2011.

[20] S. Xu, *Fracture Mechanics of Concrete*, Science Press, Beijing, China, 2011.

[21] H. Da-Hai, Y. P. Song, and G. F. Zhao, "Study on the Equivalence Strength for Crack Director of Rcc Arch Dam," *Journal of Engineering Mechanics*, 2000.

[22] X.-G. Zhang, Y.-P. Song, X.-Z. Wang, and Z.-M. Wu, "Calculation model of equivalent strength for induced crack in RCC arch dam based on double parameter fracture theory," *Dalian Ligong Daxue Xuebao/Journal of Dalian University of Technology*, vol. 45, no. 2, pp. 265–271, 2005.

[23] H.-C. Liu, Y.-P. Song, G.-J. Yao, and Z.-M. Wu, "Study of cracking for induced joints of Shapai RCC arch dam," *Journal of Dalian University of Technology*, vol. 44, no. 1, pp. 104–109, 2004.

[24] Z.-Q. Huang, X.-Z. Wang, X.-P. Shen, and Y.-P. Song, "Experiment and analysis on fracture of bilateral adjacent induced joints in RCC Arch Dam," *Journal of Hydraulic Engineering*, vol. 41, no. 2, pp. 198–204, 2010.

[25] X.-Z. Wang, Y.-P. Song, X.-G. Zhang, and Z.-M. Wu, "Study of equivalent strength for bilateral interval crack director of RCC arch dam," *Journal of Dalian University of Technology*, vol. 46, no. 2, pp. 252–256, 2006.

[26] X. Z. Wang, B. I. Zhong, L. L. Ren et al., "Influence of crack-depth ratio on RCC's nominal fracture toughness," *Concrete*, 2010.